

TrinityDNA: A Bio-Inspired Foundational Model for Efficient Long-Sequence DNA Modeling

Qirong Yang^{1*}, Yucheng Guo^{1*}, Zicheng Liu^{1,2*}, Yujie Yang¹, Qijin Yin¹, Siyuan Li^{1,2}, Shaomin Ji¹, Linlin Chao¹, Xiaoming Zhang^{1†}

¹BioMap Research, Beijing, China

²AI Lab, Research Center for Industries of the Future, Westlake University, China

Abstract

The modeling of genomic sequences presents unique challenges due to their long length and structural complexity. Traditional sequence models struggle to capture long-range dependencies and biological features inherent in DNA. In this work, we propose TrinityDNA, a novel DNA foundational model designed to address these challenges. The model integrates biologically informed components, including Groove Fusion for capturing DNA’s structural features and Gated Reverse Complement (GRC) to handle the inherent symmetry of DNA sequences. Additionally, we introduce a multi-scale attention mechanism that allows the model to attend to varying levels of sequence dependencies, and an evolutionary training strategy that progressively adapts the model to both prokaryotic and eukaryotic genomes. TrinityDNA provides a more accurate and efficient approach to genomic sequence modeling, offering significant improvements in gene function prediction, regulatory mechanism discovery, and other genomics applications. Our model bridges the gap between machine learning techniques and biological insights, paving the way for more effective analysis of genomic data. Additionally, we introduced a new DNA long-sequence CDS annotation benchmark to make evaluations more comprehensive and oriented toward practical applications.

1 Introduction

The rapid advancements in large-scale, long-sequence modeling, particularly in the realm of Natural Language Processing (NLP) (Team et al. 2023; Achiam et al. 2023), have radically transformed the way we approach complex data. Deep learning models, such as Transformers (Vaswani et al. 2017), have achieved unprecedented success in tasks that span from language translation to text generation, revolutionizing not just NLP but a variety of other fields. These models have proven their capability to capture intricate dependencies in data, providing solutions to challenges that were once considered insurmountable. With these breakthroughs in NLP, there has emerged an exciting opportunity to extend the power of sequence modeling to a completely different domain—genomics—where data shares some key similarities, such as its sequential nature.

Genomic data, particularly DNA sequences, consists of extraordinarily long strings of information that encode the

fundamental building blocks of life. Unlike the highly dense and structured data typically encountered in NLP, genomic sequences are sparse in nature, containing vast stretches of repetition and variability (Liu et al. 2024a). Despite this, they hold a rich repository of biological information that is crucial for understanding gene functions, regulatory mechanisms, and cellular processes. The ability to model DNA sequences deeply could lead to breakthrough applications in personalized medicine, genetic engineering, and the overall understanding of biological systems. However, effectively capturing the dependencies within such long, sparse sequences remains a significant challenge.

While the parallels between NLP and genomics are evident, directly applying traditional NLP models to genomic sequences proves difficult. The sparse, low-density nature of DNA sequences means that existing models often struggle to identify long-range dependencies and interpret the underlying biological structures (Mallet and Vert 2021; Zhou, Shrikumar, and Kundaje 2021). Moreover, the lack of biologically informed features in current models limits their effectiveness in genomic contexts. Many models trained on single-species data perform poorly when generalized to other species or broader biological contexts. As a result, the impact of these models on genomic research has been somewhat restricted, and their applicability to real-world challenges remains limited.

To address these issues, we introduce TrinityDNA, a novel DNA foundational model specifically designed to overcome the current limitations of genomic sequence modeling, as shown in Fig 1. TrinityDNA leverages the latest advancements in deep learning to create a model that is optimized for the unique challenges posed by DNA sequences while also incorporating key biological insights. The contributions are listed as follows:

- **Bio-inspired Design:** A multi-level architecture that is optimized for DNA sequences and leverages the Groove Fusion module and Reverse Complement (RC) fusion strategy. This design captures and exploits the unique structural properties of DNA, enabling long bi-directional genomic modeling.
- **Evolutionary Training Strategy:** A multi-species training regimen that spans a variety of organisms from prokaryotes to eukaryotes, enabling the model to generalize different genomic contexts and sequence lengths.
- **Comprehensive Large-Scale Data Integration:** Curated and integrated datasets from prominent genomic

*First three authors contribute equally.

†Corresponding author.

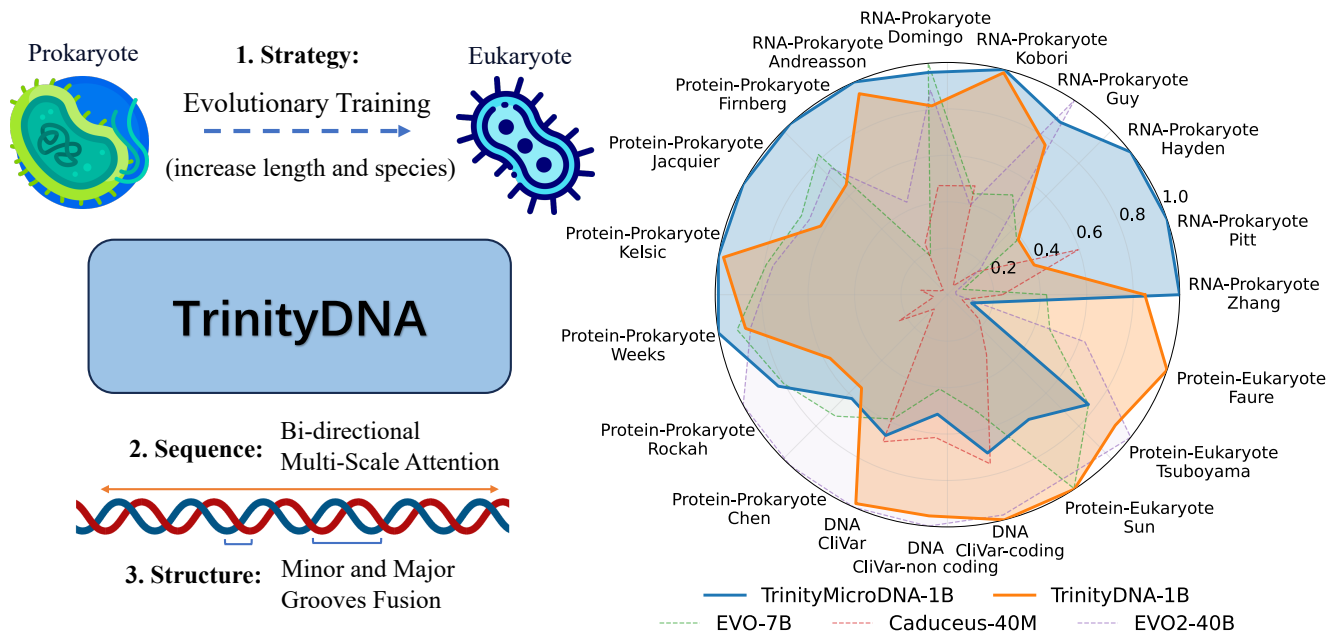


Figure 1: Overview of TrinityDNA Model: (Left) The evolutionary training strategy of TrinityDNA, progressing from prokaryotic DNA to multi-species eukaryotic DNA, and its DNA-targeted long-sequence modeling approach addressing structural features such as bidirectional complementarity and major/minor grooves. (Right) Radar chart illustrating the state-of-the-art performance on the zero-shot performance of our models versus popular models such as EVO and Caduceus.

databases such as GTDB, IMG, and RefSeq, ensuring a diverse and high-quality foundation for model training.

- **New Benchmark for Long-Sequence Inference:** We introduce a novel *CDS Annotation Benchmark* that focuses on gene-structure labeling in prokaryotic genomes, assessing both long-sequence modeling and practical annotation performance.

2 Background

DNA Terminology for Structures.

Basic Composition Deoxyribonucleic acid (DNA) is the hereditary material in most living organisms, consisting of long sequences of nucleotides. Each nucleotide comprises a phosphate group, a deoxyribose sugar, and one of four nitrogenous bases: adenine (A), thymine (T), cytosine (C), and guanine (G). A DNA sequence can be represented as a string $S = (s_1, s_2, \dots, s_N)$, where $s_i \in \{A, T, C, G\}$ and N denotes the sequence length.

Minor and Major Grooves. The double helix structure of DNA features two distinct grooves: the minor groove and the major groove. These grooves arise from the asymmetric positioning of the phosphate backbone relative to the base pairs. (1) *Major Groove*: wider and deeper, the major groove provides greater accessibility for protein binding and molecular interactions. It generally covers five to seven nucleotides. (2) *Minor Groove*: narrower and shallower, the minor groove presents a different arrangement of hydrogen bond donors and acceptors. While less accessible than the major groove, its length is three to five nucleotides.

Reverse Complement Strands. DNA molecules consist of two complementary strands running in opposite directions, a feature known as antiparallel orientation. For a DNA sequence $S = (s_1, s_2, \dots, s_N)$, its reverse complement S^R :

$$S^R = (s_N^C, s_{N-1}^C, \dots, s_1^C)$$

where s_i^C denotes the complementary base of s_i following the base-pairing rules: $A \leftrightarrow T$ and $C \leftrightarrow G$. This reverse complementarity is fundamental to DNA replication and transcription processes. Incorporating reverse complement information into computational models enhances their ability to capture symmetrical and complementary patterns, thereby improving predictions related to gene annotation and regulatory element identification.

DNA Long-Sequence Modeling

Structured State Space Models (SSMs). A prominent class of models for handling long-range dependencies is based on *Structured State Space Models (SSMs)* (Gu, Goel, and Ré 2022a, 2021, 2022b; Gupta, Schuurmans, and Ré 2022; Smith et al. 2022; Dao et al. 2022). These models emerge from discretizing a continuous-time linear system:

$$\begin{aligned} \mathbf{h}(t) &= \mathbf{A}\mathbf{h}(t) + \mathbf{B}x(t), & y(t) &= \mathbf{C}\mathbf{h}(t) + \mathbf{D}x(t), \\ \mathbf{h}_{t+1} &= \bar{\mathbf{A}}\mathbf{h}_t + \bar{\mathbf{B}}x_t, & y_{t+1} &= \mathbf{C}\mathbf{h}_t + \mathbf{D}x_t, \end{aligned}$$

where $\mathbf{h}(t)$ (or \mathbf{h}_t) is an internal state that can capture long-range dependencies in the input sequence $x(t)$ (or x_t). Through efficient convolution-based implementations of these recurrences, SSMs have shown strong performance

on very long sequences. However, conventional SSMs do not explicitly adapt their parameters to specific tokens or positions, which may limit expressivity for tasks such as DNA sequence modeling. Therefore, a line of SSMs are designed for long-sequence DNA.

HyenaDNA (EVO). *HyenaDNA* (Poli, Suteu et al. 2023) is an SSM variant, a decoder-style model capable of handling long genomic sequences (e.g., hundreds of thousands of tokens). It leverages the *Hyena* operator, which replaces traditional attention with a fast convolution-based mechanism. Concretely, HyenaDNA blocks compute a Toeplitz convolution filter on projected input tokens, allowing processing of very large contexts (in $\mathcal{O}(L \log L)$ time) without the quadratic cost typically associated with attention.

Caduceus (MambaDNA). *MambaDNA* (Schiff et al. 2024)—also referred to as *Caduceus*—builds on the selective SSM approach of Mamba and incorporates *reverse-complement symmetry*, a core property of DNA sequences. In standard Mamba, the module processes sequences in a single direction. MambaDNA extends this design in two ways: (1) **BiMamba**: Instead of only left-to-right processing, BiMamba applies the Mamba block twice. (2) **RC Equivariance**: MambaDNA explicitly enforces RC symmetry by taking a sequence and its RC as inputs to the same SSM-based module. See more details in Appendix E.

3 TrinityDNA: Sequence, Structure, and Strategy for DNA Modeling

Preliminaries

Lost in the locality. While SSMs theoretically excel at handling long sequences, they inherently exhibit a *locality bias* (Wang et al. 2024). This issue is exacerbated in DNA sequence modeling, where dependencies across vast genomic regions must be captured to enable accurate biological interpretation. Specifically, in genomic data, long-range dependencies often span tens of thousands or even hundreds of thousands of base pairs. Existing models, such as SSMs, typically focus on local dependencies due to computational challenges in processing long sequences. Consequently, our empirical results in Figure 2 demonstrate that

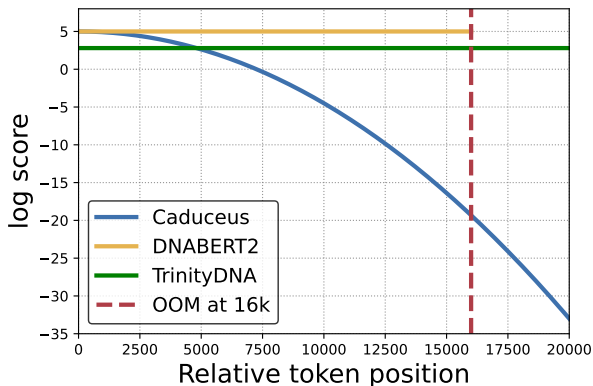


Figure 2: Comparison of log influential scores $\log |\partial y_t / \partial x_s|$ versus distance $(t - s)$ on HG-38 (Nguyen et al. 2023).

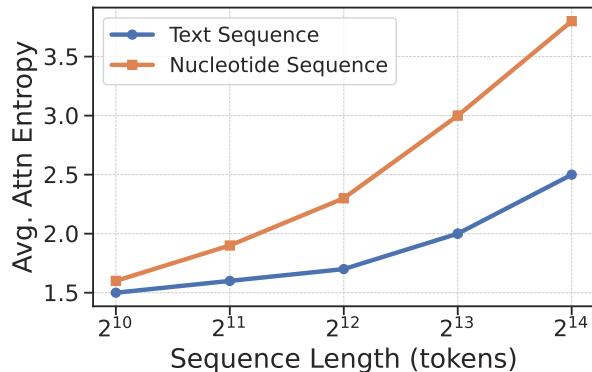


Figure 3: Average attention entropy of full self-attention models as sequence length increases.

the SSM-based model (Caduceus) lost their focus as the sequence length increased, while the full-attention-based model (DNABERT2) suffered from heavy computation. These limitations hinder modern DNA foundation models’ ability to fully capture the inherent complexities of DNA sequences and their interconnections across genomic regions.

Over-smoothing in long attention. As sequences grow in training, full self-attention “flattens out”: attention scores converge toward a uniform, high-entropy distribution in Figure 3, so every token is weighted almost equally, and useful signals vanish. This over-smoothing affects low-density data—images, DNA, and the hardest—where informative tokens are sparse and far apart. In shorter windows, the same model still shows specialized heads, e.g., retrieval vs. induction (Xiao et al. 2024), but that diversity collapses at the kilobase scale. These findings motivate a multi-window, multi-head scheme that combines narrow local windows with broader global ones to reduce entropy and maintain head specialization. Detailed settings refers to the Appendix.

Groove Fusion Module

To account for the minor and major grooves in DNA sequences, we propose a Groove Fusion module that combines convolutional operations of varying kernel sizes. These grooves have distinct structural and functional roles in DNA, with the major groove offering greater accessibility for protein binding and the minor groove being involved in different molecular interactions. To model these differences, we perform tokenization on the DNA sequence using three convolutional kernels of sizes 3, 5, and 7. This multi-scale convolution approach enables the model to focus on different spatial features across the sequence, effectively capturing the structural nuances associated with the two grooves.

Formally, the Groove Fusion process can be defined as:

$$\text{GrooveFusion}(S) = \sum_{k \in \{3, 5, 7\}} \text{GELU}(\text{Conv}_k(S))$$

where Conv_k represents the convolution operation with kernel size k , and S is the input DNA sequence. The output of each convolution operation is fused to capture the multi-scale contextual information necessary for interpreting the structural variations between the major and minor grooves.

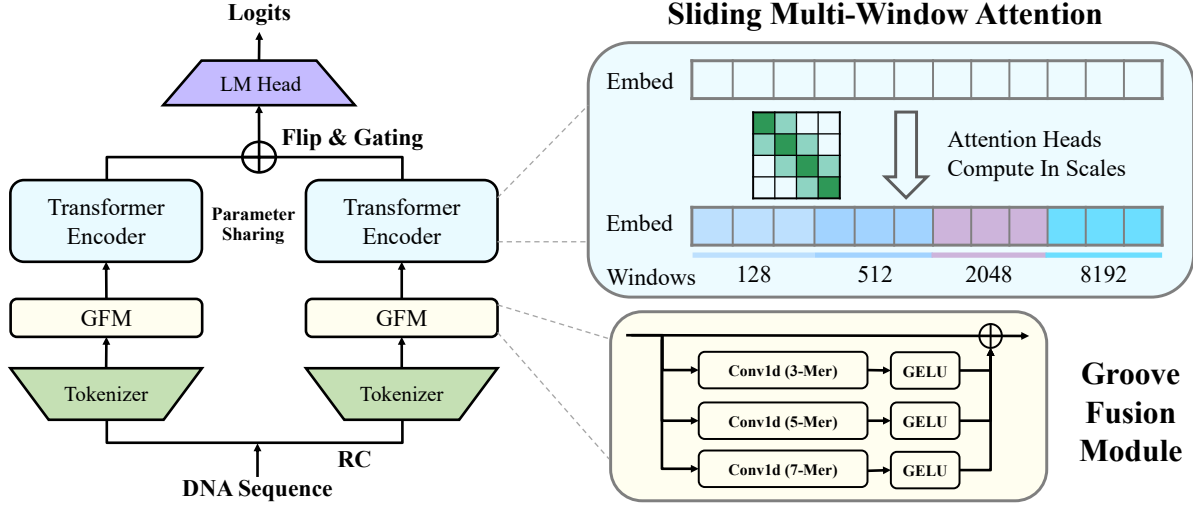


Figure 4: Model Architecture of TrinityDNA: The model integrates DNA sequences and structural features by considering its grooves and reverse complementary sequence with shared parameters.

Sliding Multi-Window Attention

To mitigate locality bias and attention oversmoothing, we revisit the design of Multi-Head Attention (MHA), focusing on varying attention window sizes across heads. In traditional MHA, each head typically attends to the entire sequence using a fixed attention window, which can limit the model’s ability to capture dependencies at different scales. To address this, we introduce a multi-scale attention grouping strategy named SMWA. In this approach, we assign different attention heads to capture dependencies at different scales in the DNA sequence, enabling the model to specialize in local or global dependencies, depending on the feature scale. Formally, we define the window sizes for each attention head h as $L_h \in \mathbb{N}$, with L_h representing the length of the attention window for head h . For head h , the attention mechanism is computed using a sliding window of size L_h over the sequence, allowing the model to focus on scales:

$$\text{Attn}_h(S_i) = \text{Softmax} \left(\frac{Q_h(i)K_h(i + [-L_h, L_h])^T}{\sqrt{d_k}} \right) V_h(i + [-L_h, L_h])$$

where $Q_h \in \mathbb{R}^{N \times d_k}$ is the query matrix for head h , $K_h \in \mathbb{R}^{N \times d_k}$ is the key matrix, $V_h \in \mathbb{R}^{N \times d_v}$ is the value matrix, N is the sequence length, and d_k and d_v are the dimensionality of the key and value vectors, respectively. i is the index of the sequence, and $[-L_h, L_h]$ represents the range of indices for the sliding window around i . This enables each head to specialize in attending to either short-range or long-range dependencies by adjusting L_h . The final output of the multi-head attention layer is the concatenation of all heads’ outputs, followed by a linear transformation:

$$\text{SMWA}(S) = \text{Concat}(\text{Attn}_1, \text{Attn}_2, \dots, \text{Attn}_H)W_O$$

where $W_O \in \mathbb{R}^{d_{\text{out}} \times d_{\text{in}}}$ is a learned output weight matrix, H is the number of attention heads, and d_{out} is the output dimensionality. This multi-scale attention mechanism allows

the model to simultaneously capture both local and global dependencies by allocating different heads to focus on different sequence scales. Thus, shorter sequences can be captured by heads with smaller windows, while longer-range dependencies can be modeled by heads with larger windows, enabling the model to capture the hierarchical nature of DNA sequences better.

Gated Reverse Complement

To leverage the reverse complementarity inherent in DNA sequences, we introduce a novel Gated Reverse Complement (GRC) mechanism. This mechanism employs a shared Transformer module to process both the forward and reverse complement sequences in parallel. The reverse complement of a DNA sequence $S = (s_1, s_2, \dots, s_N)$ is defined as $S^R = (s_N^C, s_{N-1}^C, \dots, s_1^C)$, where s_i^C denotes the complementary base of s_i (with base-pairing rules $A \leftrightarrow T$, $C \leftrightarrow G$). The GRC mechanism works by feeding both the forward and reverse complement sequences into a shared SMWA-equipped Transformer network f_θ , where the outputs are gated using a linear gating mechanism to combine the two representations effectively. The final layer is:

$$\text{Output} = \text{GRC}(S, S^R) = f_\theta(S) + \sigma(W_G \cdot f_\theta(\text{Flip}(S^R)))$$

where W_G are learned weights, σ represents the identity function, and the Flip operator means to reverse the sequence in the original order. This allows the model to learn the representations of both sides simultaneously.

Evolutionary Training Strategy

The Evolutionary Training Strategy (ETS) approach leverages a two-stage, evolution-inspired training strategy to progressively address the varying complexities of genomic data. In the first stage, the model is trained on prokaryotic genomes, which are relatively straightforward in terms of their regulatory architectures (Xu and Jin 2006; Nguyen

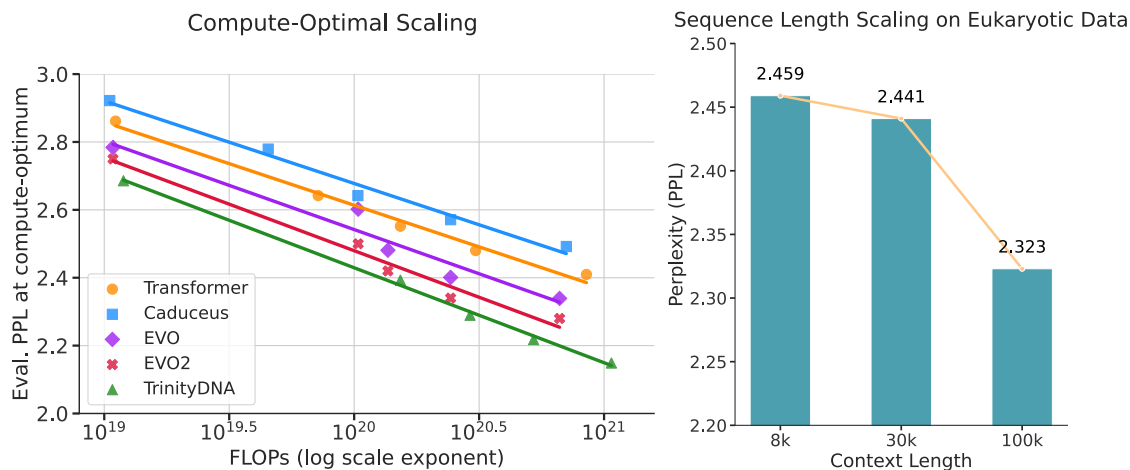


Figure 5: **Scaling Behaviors of Our Proposed Model.** (Left) Evaluation perplexity (PPL) against total FLOPs across multiple architectures, showing consistent improvements to various baselines. (Right) Impact of increasing context length (8k, 30k, 100k) on a eukaryotic dataset, where PPL steadily decreases with longer context windows.

et al. 2024). Through this foundational phase, the model captures essential DNA sequence motifs and organizational patterns. Subsequently, the second stage introduces eukaryotic genomes, known for their intron-exon structures and gene lengths that can span tens of kilobases (Dalla-Torre et al. 2024). Alongside this transition, the model’s context window is enlarged from 8K to 100K base pairs, accommodating multiple co-expressed genes and regulatory elements.

4 Experiments

Pre-training

Data. We adopt masked language modeling (MLM) (Devlin et al. 2018) and character-level tokenization for all our DNA models. Following our *Evolutionary training* strategy, we conduct pre-training in two phases: Stage 1 (Short-Sequence Pre-training): We use prokaryotic (bacterial and archaeal) DNA data from the OpenGenome dataset introduced in (Nguyen et al. 2024), training on sequences of length 8k to learn fundamental nucleic acid patterns in shorter contexts. Stage 2 (Multi-species Post-training): We then continue pre-training on a multi-species collection, the Multispecies dataset, presented in (Dalla-Torre et al. 2024). The sequences in this stage can be as long as 100k, spanning archaeobacteria, fungi, vertebrate genomes, and more. This step exposes the model to a rich spectrum of evolutionary signals, enabling it to handle much longer contexts and to capture the diverse structural intricacies of eukaryotic DNA. Hence, we propose two main models, *TrinityMicroDNA* and *TrinityDNA*, each with 1 billion (1B) parameters. The former is trained solely on prokaryotic data, while the latter builds upon the former by post-training on eukaryotic data. By transitioning from bacterial genomes to longer eukaryotic genomes, our method achieves broad coverage of genomic features across scales. More details in Appendix A.

Scaling Laws. Figure 5 illustrates three key aspects of our model’s scaling behavior across parameter sizes, pre-training context lengths (8k, 30k, 100k). (Left) We plot the

compute-perplexity frontier against total FLOPs for several architectures, demonstrating that our approach consistently outperforms baseline methods (Transformer, Caduceus, EVO, and EVO2) at every compute level in different parameter sizes (6M to 1B). (Right) We examine the effect of increasing context window sizes on a eukaryotic benchmark, finding a steady drop in perplexity when moving from 8k to 30k, and a further substantial improvement at 100k.

Ablation Study and Analysis

(1) Effectiveness. Table 1 shows that GFM consistently lowers perplexity by modeling the spatial ‘groove’ features of DNA sequences. Likewise, incorporating GRC (captures reverse-complement patterns) yields a notable drop in PPL, reflecting the importance of complementary-strand information. Meanwhile, SMWA enables multi-scale context handling, trading off some computational overhead for competitive perplexity across local and longer-range dependencies. Although SMWA incurs some performance loss, it is still evident that it saves resources for long sequence training.

(2) Efficiency. The left panel of Figure 6 contrasts token-throughput as we sweep both sequence length and micro-batch size on 1B scale. Across every setting, *TrinityDNA* remains clearly at the top, retaining more than 80% of its short-sequence throughput even at 64k tokens. This robustness stems from its sliding multi-window attention and optimized fused kernels, which maintain memory traffic at a

Components	W/O	W	W/O	W
GRC	2.731	2.599 (-0.132)	-	-
GFM	2.599	2.534 (-0.065)	-	-
SMWA	2.534	2.544 (+0.010)	64.5	44.5 (-31%)

Table 1: Effect of components on pre-training perplexity (left side) and computational cost (left side, TFLOPs).

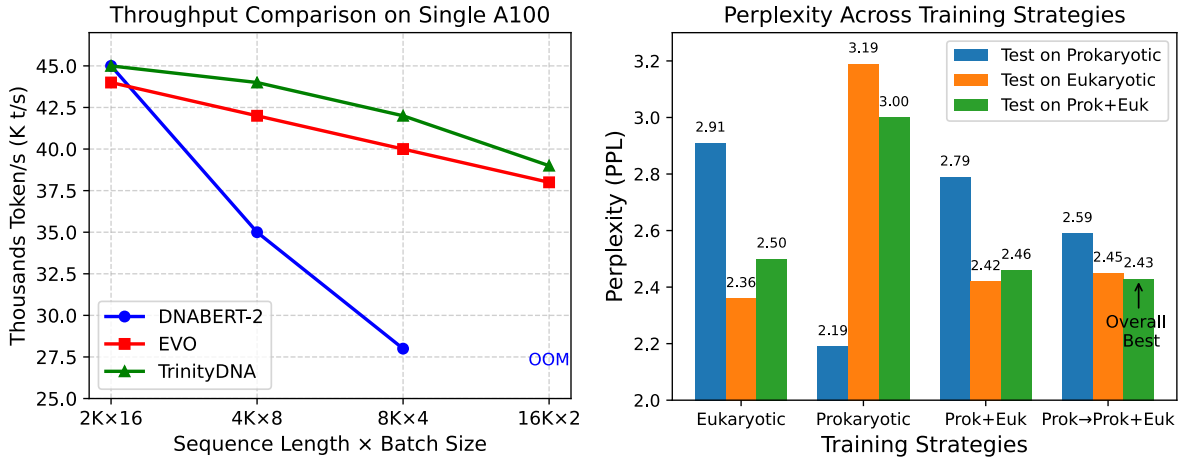


Figure 6: Comprehensive ablation study and efficiency analysis on TrinityDNA.

Tasks	DNABERT 86M	NT 2.5B	DNABERT2 117M	Caduceus 40M	HyenaDNA 1.6M	TrinityDNA 1B
H3	0.731 \pm 0.015	0.788 \pm 0.012	0.783 \pm 0.014	0.799 \pm 0.029	0.779 \pm 0.037	0.814 \pm 0.014
H3K14ac	0.401 \pm 0.018	0.562 \pm 0.015	0.526 \pm 0.019	0.541 \pm 0.212	0.612 \pm 0.065	0.694 \pm 0.016
H3K36me3	0.473 \pm 0.017	0.620 \pm 0.012	0.569 \pm 0.015	0.609 \pm 0.109	0.613 \pm 0.041	0.692 \pm 0.014
H3K4me1	0.414 \pm 0.012	0.553 \pm 0.011	0.505 \pm 0.015	0.488 \pm 0.102	0.512 \pm 0.024	0.611 \pm 0.015
H3K4me2	0.323 \pm 0.014	0.365 \pm 0.010	0.311 \pm 0.013	0.388 \pm 0.101	0.455 \pm 0.095	0.480 \pm 0.013
H3K4me3	0.278 \pm 0.015	0.403 \pm 0.011	0.363 \pm 0.014	0.440 \pm 0.202	0.549 \pm 0.056	0.522 \pm 0.015
H3K79me3	0.612 \pm 0.013	0.647 \pm 0.010	0.674 \pm 0.012	0.676 \pm 0.026	0.672 \pm 0.048	0.741 \pm 0.014
H3K9ac	0.512 \pm 0.015	0.560 \pm 0.013	0.556 \pm 0.017	0.604 \pm 0.048	0.581 \pm 0.061	0.662 \pm 0.014
H4	0.793 \pm 0.012	0.817 \pm 0.015	0.807 \pm 0.011	0.789 \pm 0.020	0.763 \pm 0.044	0.829 \pm 0.012
H4ac	0.372 \pm 0.016	0.491 \pm 0.018	0.504 \pm 0.019	0.525 \pm 0.240	0.564 \pm 0.038	0.632 \pm 0.013
Human TF	0.642 \pm 0.012	0.633 \pm 0.015	0.701 \pm 0.020	-	-	0.714 \pm 0.009
Mouse TF	0.564 \pm 0.018	0.670 \pm 0.014	0.680 \pm 0.015	-	-	0.786 \pm 0.012
Promoter	0.768 \pm 0.015	0.799 \pm 0.012	0.774 \pm 0.019	-	-	0.803 \pm 0.012
Splice Recon.	0.841 \pm 0.010	0.894 \pm 0.014	0.850 \pm 0.020	-	-	0.927 \pm 0.009
Virus Covid	0.555 \pm 0.017	0.730 \pm 0.012	0.710 \pm 0.014	-	-	0.706 \pm 0.015
Overall Avg	0.552	0.636	0.621	0.586	0.610	0.708

Table 2: GUE Benchmark performance comparison. Metrics are single/multi-label binary classification (MCC).

nearly constant level as the context grows.

(3) Training Strategies. The right plot in Figure 6 shows a comprehensive ablation study separating the contributions of dataset size and evolutionary training strategy. The table shows perplexity scores across different model configurations. Key finding: Models initialized with weights from prokaryotic pre-training and then fine-tuned on combined data show better performance than models trained from scratch on the combined dataset. This validates both the importance of large, diverse datasets and our EST.

Downstream Tasks

We employ TrinityMicroDNA and TrinityDNA with 1B parameters as our base model for downstream evaluation, and we use LoRA tuning except for the zero-shot task.

GUE Benchmark We evaluate our models on a comprehensive Genomic Understanding Evaluation (GUE) benchmark comprising tasks from *Genomics Benchmark* (Zhou

et al. 2023) and *Nucleotide Transformer* tasks (Dalla-Torre et al. 2024) by standard LoRA fine-tuning (Hu et al. 2021). For baselines, results are used in the original paper.

Results In Table 2, we compare models DNABERT, Nucleotide Transformer (NT), DNABERT2, and TrinityDNA. Overall, ours outperforms prior methods across many metrics. We observe large improvements in tasks that demand recognition of extended promoter regions or higher-order structural features, aligning with our architectural design for multi-window attention and GRC-based reverse complement awareness.

Zero-shot Performance We evaluated our two 1B models on 19 zero-shot downstream tasks—covering DNA pathogenicity (ClinVar), seven RNA DMS benchmarks and fifteen protein-fitness benchmarks across prokaryotic and eukaryotic (Table 3). The prokaryote-focused TrinityMicroDNA-1B dominates the prokaryotic regime, winning 8 of 13 prokaryotic tasks and attaining the high-

Task Type	Task	TrinityMicroDNA	TrinityDNA	EVO	EVO2	EVO2	Caduceus
	# Params	1B	1B	7B	40B	1B	40M
RNA DMS (Prokaryote)	Zhang	0.560	<u>0.476</u>	0.239	0.021	0.152	0.133
	Pitt	0.294	0.116	0.021	0.011	0.040	<u>0.175</u>
	Hayden	0.365	<u>0.141</u>	0.138	0.065	0.010	0.059
	Guy	0.370	0.321	0.214	0.417	0.354	0.019
	Kobori	0.569	<u>0.561</u>	0.255	0.226	0.317	0.275
	Domingo	0.438	0.372	0.456	0.403	0.315	0.215
	Andreasson	0.292	<u>0.276</u>	0.053	0.127	0.036	0.070
Protein DMS (Prokaryote)	Firnberg	0.673	0.433	0.552	0.499	<u>0.621</u>	0.018
	Jacquier	0.659	0.409	0.471	0.446	<u>0.529</u>	0.023
	Kelsic	0.406	0.397	0.321	0.309	0.463	0.047
	Weeks	0.573	0.505	0.526	0.492	<u>0.561</u>	0.034
	Rockah	0.592	0.411	0.574	0.715	<u>0.657</u>	0.168
	Chen	0.383	0.344	0.448	0.630	<u>0.534</u>	0.053
DNA	ClinVar	0.629	<u>0.933</u>	0.555	0.950	0.927	0.657
	ClinVar-non coding	0.503	<u>0.931</u>	0.397	0.974	0.920	0.601
	ClinVar-coding	0.654	0.930	0.484	<u>0.910</u>	0.898	0.699
Protein DMS (Eukaryote)	Sun	0.202	<u>0.315</u>	0.314	0.295	0.334	0.097
	Tsuboyama	0.595	0.708	0.595	0.773	<u>0.717</u>	0.134
	Faure	0.067	0.609	0.284	0.381	<u>0.482</u>	0.041
Average Performance (Prokaryote)		0.475	<u>0.366</u>	0.328	0.335	0.353	0.099
Average Performance (Eukaryote)		0.404	0.699	0.415	0.667	<u>0.670</u>	0.314

Table 3: Zero-shot performance across DNA, RNA, and protein DMS tasks. ClinVar tasks are binary classification (AUC); others are RNA/protein fitness regression (Spearman).

Category	Models	Exact Match			75% Match		
		Recall	Precision	F1	Recall	Precision	F1
Pre-trained Models	TrinityMicroDNA-1B	0.775	0.740	0.754	0.826	0.788	0.803
	TrinityMicroDNA-470M	0.743	0.623	0.692	0.803	0.693	0.755
	TrinityMicroDNA-6M	0.592	0.333	0.488	0.723	0.445	0.524
	Caduceus-40M	0.149	0.148	0.140	0.194	0.189	0.180
Classical Pipelines	Prodigal	0.832	0.666	0.725	0.909	0.765	0.829
	GENSCAN	0.721	0.681	0.702	0.810	0.774	0.799
	Glimmer	0.704	0.663	0.688	0.802	0.760	0.780

Table 4: Results of CDS Annotation Benchmark on the filtered *RefSeq* test set.

est prokaryotic average (0.475), whereas the multi-species TrinityDNA-1B excels on eukaryotic protein-fitness prediction, delivering the top score and the highest eukaryotic average (0.699), even surpassing the 40B EVO2 model (0.667). TrinityDNA also excels in state-of-the-art DNA pathogenicity performance, leading in CliVar-coding and ranking second overall. These complementary strengths underscore the benefit of ETS, and a UMAP projection of genome-level embeddings for ten representative clades (Appendix D) reveals clear taxonomic clustering, indicating that both models learn rich species signals without fine-tuning.

CDS Annotation Benchmark We also introduce a novel CDS Annotation Benchmark, aiming to assess long-sequence inference capabilities, practical utility for gene annotation in real-world genomes. From RefSeq, we collect all prokaryotic reference genomes and parse the GenBank annotation files for gene positions/types. This yields token-level labels indicating whether each token belongs to a coding sequence (CDS) with 20k sequence length and, if so,

in which strand/direction it is transcribed. The detailed data statistics are described in Appendix D.

Results The results are shown in Table 4. While Prodigal shows strong recall performance, TrinityMicroDNA-1B delivers the best precision and F1 scores for exact matches, highlighting the model’s strong generalization capabilities across diverse datasets compared to classical pipelines.

5 Conclusion

We present TrinityDNA, a foundational DNA model that integrates biologically inspired modules—*Groove Fusion* and *Gated Reverse Complement*—alongside a *multi-scale attention mechanism* to capture scales of genomic context effectively, built upon an ETS that transitions from prokaryotic to eukaryotic genomes. TrinityDNA gains strong generalization for diverse genomic prediction tasks. We also introduce the *CDS Annotation Benchmark*, which evaluates coding sequence identification across organisms and provides a realistic standard for genome-scale annotation.

References

- Achiam, J.; Adler, S.; Agarwal, S.; Ahmad, L.; Akkaya, I.; Aleman, F. L.; Almeida, D.; Altenschmidt, J.; Altman, S.; Anadkat, S.; et al. 2023. Gpt-4 technical report. *arXiv preprint arXiv:2303.08774*.
- Benson, D. A.; Cavanaugh, M.; Clark, K.; Karsch-Mizrachi, I.; Lipman, D. J.; Ostell, J.; and Sayers, E. W. 2012. GenBank. *Nucleic Acids Research*, 41(D1):D36–D42.
- Dalla-Torre, H.; Gonzalez, L.; Mendoza-Revilla, J.; Carranza, N. L.; Grzywaczewski, A. H.; Oteri, F.; Dallago, C.; Trop, E.; de Almeida, B. P.; Sirelkhatim, H.; et al. 2023. The nucleotide transformer: Building and evaluating robust foundation models for human genomics. *bioRxiv*, 2023–01.
- Dalla-Torre, H.; Gonzalez, L.; Mendoza-Revilla, J.; Lopez Carranza, N.; Grzywaczewski, A. H.; Oteri, F.; Dallago, C.; Trop, E.; de Almeida, B. P.; Sirelkhatim, H.; et al. 2024. Nucleotide Transformer: building and evaluating robust foundation models for human genomics. *Nature Methods*, 1–11.
- Dao, T.; Jain, S.; Rudra, A.; and Ré, C. 2022. Hungry Hungry Hippos: Towards Language Model Scaling via Back-propagation in Space. *arXiv preprint arXiv:2212.14052*.
- Devlin, J.; Chang, M.-W.; Lee, K.; and Toutanova, K. 2018. Bert: Pre-training of deep bidirectional transformers for language understanding. *arXiv preprint arXiv:1810.04805*.
- Dreos, R.; Ambrosini, G.; Perier, R. C.; and Bucher, P. 2013. EPD and EPDnew, high-quality promoter resources in the next-generation sequencing era. *Nucleic Acids Research*.
- Gu, A.; Goel, K.; and Ré, C. 2021. Combining Recurrent, Convolutional, and Continuous-time Models with Linear State-Space Layers. *arXiv preprint arXiv:2103.10897*.
- Gu, A.; Goel, K.; and Ré, C. 2022a. Efficiently Modeling Long Sequences with Structured State Spaces. In *International Conference on Learning Representations (ICLR)*.
- Gu, A.; Goel, K.; and Ré, C. 2022b. Parameterization and Initialization of Diagonal State Spaces for Sequence Modeling. *arXiv preprint arXiv:2208.04933*.
- Gupta, H.; Schuurmans, D.; and Ré, C. 2022. Diagonally-Scalable Structured State Space Models for Long Sequence Modeling. *arXiv preprint arXiv:2211.07225*.
- Hu, E. J.; Shen, Y.; Wallis, P.; Allen-Zhu, Z.; Li, Y.; Wang, S.; Wang, L.; and Chen, W. 2021. LoRA: Low-Rank Adaptation of Large Language Models. *arXiv:2106.09685*.
- Ji, Y.; Zhou, Z.; Liu, H.; and Davuluri, R. V. 2021. DNABERT: pre-trained Bidirectional Encoder Representations from Transformers model for DNA-language in genome. *Bioinformatics*, 37(15): 2112–2120.
- Khare, S.; Gurry, C.; Freitas, L.; Kelly, B. B.; Maurer-Stroh, S.; et al. 2021. GISAID’s role in pandemic response. *China CDC Weekly*, 3(49):1049–1051.
- Li, S.; Wang, Z.; Liu, Z.; Wu, D.; Tan, C.; Zheng, J.; Huang, Y.; and Li, S. Z. 2024. VQDNA: Unleashing the Power of Vector Quantization for Multi-Species Genomic Sequence Modeling. In *International Conference on Machine Learning (ICML)*.
- Liu, Z.; Li, J.; Li, S.; Zang, Z.; Tan, C.; Huang, Y.; Bai, Y.; and Li, S. Z. 2024a. GenBench: A Benchmarking Suite for Systematic Evaluation of Genomic Foundation Models. *arXiv:2406.01627*.
- Liu, Z.; Li, S.; Wang, L.; Wang, Z.; Liu, Y.; and Li, S. Z. 2024b. Short-Long Convolutions Help Hardware-Efficient Linear Attention to Focus on Long Sequences. *arXiv:2406.08128*.
- Liu, Z.; Wang, L.; Li, S.; Wang, Z.; Lin, H.; and Li, S. Z. 2024c. LongVQ: Long Sequence Modeling with Vector Quantization on Structured Memory. *arXiv:2404.11163*.
- Mallet, V.; and Vert, J.-P. 2021. Reverse-complement equivariant networks for DNA sequences. *Advances in Neural Information Processing Systems*, 34: 13511–13523.
- Nebrao, M. J.; Kung, V. T.; Rowe, K.; Amaral, G. R.; Azad, R. K.; and Cambray, G. 2021. No one tool to rule them all: prokaryotic gene prediction tool annotations are highly dependent on the organism of study. *Bioinformatics*.
- Nguyen, E.; Poli, M.; Durrant, M. G.; Kang, B.; Katrekar, D.; Li, D. B.; Bartie, L. J.; Thomas, A. W.; King, S. H.; Brix, G.; Sullivan, J.; Ng, M. Y.; Lewis, A.; Lou, A.; Ermon, S.; Baccus, S. A.; Hernandez-Boussard, T.; Ré, C.; Hsu, P. D.; and Hie, B. L. 2024. Sequence modeling and design from molecular to genome scale with Evo. *Science*, 386(6723): ead09336.
- Nguyen, E.; Poli, M.; Faizi, M.; Thomas, A.; Birch-Sykes, C.; Wornow, M.; Patel, A.; Rabideau, C.; Massaroli, S.; Bengio, Y.; et al. 2023. Hyenadna: Long-range genomic sequence modeling at single nucleotide resolution. *arXiv preprint arXiv:2306.15794*.
- Notin, P.; Kollasch, A.; Ritter, D.; Van Niekerk, L.; Paul, S.; Spinner, H.; Rollins, N.; Shaw, A.; Orenbuch, R.; Weitzman, R.; et al. 2023. Proteingym: Large-scale benchmarks for protein fitness prediction and design. *Advances in Neural Information Processing Systems*, 36: 64331–64379.
- Poli, M.; Suteu, I.; et al. 2023. Hyena: A Quasi-Attention Approach to Long-Range Language Modeling. *arXiv preprint arXiv:2302.10866*.
- Schiff, Y.; Kao, C.-H.; Gokaslan, A.; Dao, T.; Gu, A.; and Kuleshov, V. 2024. Caduceus: Bi-Directional Equivariant Long-Range DNA Sequence Modeling. *arXiv:2403.03234*.
- Smith, S.; Gu, A.; Roberts, D. A.; and Ré, C. 2022. Simplified State Space Layers for Sequence Modeling. *arXiv preprint arXiv:2209.12951*.
- Stamatoyannopoulos, J. A.; Snyder, M.; Hardison, R.; Ren, B.; Gingeras, T.; Bernstein, B. E.; et al. 2012. An encyclopedia of mouse DNA elements (Mouse ENCODE). *Genome Biology*, 13(8):418.
- Team, G.; Anil, R.; Borgeaud, S.; Wu, Y.; Alayrac, J.-B.; Yu, J.; Soricut, R.; Schalkwyk, J.; Dai, A. M.; Hauth, A.; et al. 2023. Gemini: a family of highly capable multimodal models. *arXiv preprint arXiv:2312.11805*.
- The ENCODE Project Consortium. 2012. An integrated encyclopedia of DNA elements in the human genome. *Nature*, 489(7414):57–74.
- Vaswani, A.; Shazeer, N.; Parmar, N.; Uszkoreit, J.; Jones, L.; Gomez, A. N.; Kaiser, Ł.; and Polosukhin, I. 2017. Attention is all you need. *Advances in neural information processing systems*, 30.
- Wang, P.; Cai, R.; Wang, Y.; Zhu, J.; Srivastava, P.; Wang, Z.; and Li, P. 2024. Understanding and Mitigating Bottlenecks of State Space Models through the Lens of Recency and Over-smoothing. *arXiv:2501.00658*.

Wang, R.; Bai, X.; and Chen, K. 2019. SpliceFinder: Differential splicing detection using RNNs. *Bioinformatics*, 35(14):2373–2380.

Xiao, G.; Tang, J.; Zuo, J.; Guo, J.; Yang, S.; Tang, H.; Fu, Y.; and Han, S. 2024. DuoAttention: Efficient Long-Context LLM Inference with Retrieval and Streaming Heads. *arXiv*.

Xu, Z.; and Jin, L. 2006. Genome-wide average gene length is highly conserved but recombination rate varies among prokaryotes and eukaryotes.

Zaheer, M.; Guruganesh, G.; Dubey, K. A.; Ainslie, J.; Alberti, C.; Ontanon, S.; Pham, P.; Ravula, A.; Wang, Q.; Yang, L.; et al. 2020. Big bird: Transformers for longer sequences. *Advances in neural information processing systems*, 33: 17283–17297.

Zhou, H.; Shrikumar, A.; and Kundaje, A. 2021. Towards a better understanding of reverse-complement equivariance for deep learning models in regulatory genomics. *BioRxiv*, 2020.

Zhou, Z.; Ji, Y.; Li, W.; Dutta, P.; Davuluri, R.; and Liu, H. 2023. Dnabert-2: Efficient foundation model and benchmark for multi-species genome. *arXiv preprint arXiv:2306.15006*.

A Appendix of TrinityDNA

B Experimental Setups

In this appendix, we offer comprehensive details regarding the experimental setup for our research.

Hardware Configuration We conduct our experiments on a cluster of 31 host machines. Each machine is equipped with 8 A100 GPUs, providing substantial parallel computing power. The total number of CPU cores available across the cluster is 128, and the total memory amounts to 1007 GB. The operating system used is Ubuntu with the kernel version 5.4.0 - 139 - generic. Additionally, we utilize RDMA (Remote Direct Memory Access) technology to enhance data transfer efficiency. The DCGM (Data Center GPU Manager) drive version is 525.147.05.

Details for Log Influential Score Analysis

The analysis of **log influential scores** was designed to quantitatively measure how the influence of an input token on an output token diminishes with increasing distance between them. This helps to empirically visualize the locality bias of different model architectures.

- Models and Dataset:** We utilized the official pretrained checkpoints for the SSM-based model Caduceus-Phage and the full-attention model DNABERT2. The analysis was conducted on the human reference genome, HG-38.
- Sequence Sampling:** We randomly selected a contiguous sequence of 20,000 base pairs from the HG-38 genome to serve as the input for the models.
- Influence Calculation:** The influential score is defined as the gradient of a model’s output with respect to its input, specifically $|\partial y_t / \partial x_s|$. This value quantifies the extent to which a change in the input token at position s affects the model’s prediction at position t .
 - To compute this, we performed a forward pass with the 20k-token sequence.
 - We then used backpropagation to calculate the gradients of the output logits (y_t) with respect to the input embeddings (x_s) for a chosen target position t near the end of the sequence.
 - We computed the absolute value of these gradients and took their logarithm, yielding the log influential score, $\log |\partial y_t / \partial x_s|$.
- Plotting:** The scores were plotted against the relative distance between the input and output tokens, $(t - s)$. The curve for each model represents the average scores over multiple runs with different randomly sampled sequences. The vertical dashed line labeled “OOM at 16k” indicates the point at which DNABERT2 failed to process the sequence due to an out-of-memory error, a known limitation of its quadratic attention mechanism.

Details for Average Attention Entropy Analysis

The experiment on **average attention entropy** was conducted to demonstrate the “oversmoothing” phenomenon in standard Transformer models, where attention distributions become increasingly uniform as sequence lengths grow.

- Model Architecture:** We constructed a standard two-layer Transformer encoder with full self-attention. The model was intentionally kept simple to isolate the effect of sequence length on the attention mechanism itself, without confounding factors from more complex architectures.
- Datasets and Training:** We trained two separate instances of this model from scratch:
 - One on a large corpus of English text from **Wikipedia (Text Sequence)**.
 - Another on genomic data from the **HG-38 reference genome (Nucleotide Sequence)**.

This dual-dataset approach allowed us to compare the oversmoothing effect across different data modalities.

- Entropy Calculation:** After training, the models were evaluated on sequences of varying lengths, from 2^{10} (1024) to 2^{14} (16384) tokens.
 - For each input sequence, we extracted the attention probability distributions, p , from every attention head at every position.
 - We then calculated the **Shannon entropy** for each distribution using the formula $H(p) = -\sum_i p_i \log_2 p_i$. A higher entropy value indicates a more uniform (or “smoother”) distribution, while a lower entropy value suggests a more focused, spiky distribution.
 - The final “**Avg. Attn Entropy**” value for each sequence length shown on the y-axis is the mean entropy calculated across all attention heads and all token positions in the sequence.
- Plotting:** The chart plots the average attention entropy as a function of sequence length. The x-axis is on a logarithmic scale (2^N) to clearly show the trend across several orders of magnitude in sequence length.

Training Framework Our training framework is built upon the Megatron and DeepSpeed training frameworks, integrating FlashAttention to accelerate attention computation. It supports DeepSpeed-Ulysess for efficient memory management and large-scale model training, while also incorporating Pipeline Parallelism, Model Parallelism, and Data Parallelism (4D). This unique combination allows us to train models with longer context lengths and more complex architectures without compromising performance. Notably, while DeepSpeed-Ulysess currently does not support Pipeline Parallelism, our framework has successfully integrated both DeepSpeed-Ulysess and Pipeline Parallelism alongside Model and Data Parallelism, enabling a highly scalable and efficient 4D parallelism approach for state-of-the-art model training. For our experiments, we build upon the PyTorch and PyTorch Lightning frameworks, which are widely recognized for their flexibility and efficiency in deep learning research. Our model adopts a Transformer encoder-only architecture. We incorporate several advanced techniques within this architecture:

Activation Function : We use the GELU (Gated Gaussian Error Linear Unit) activation function, which has shown superior performance in handling complex data patterns compared to traditional activation functions.

Normalization Layers : To stabilize the training process, we employ DeepNorm and LayerNorm. DeepNorm helps in mitigating the vanishing and exploding gradient problems, especially in deep neural networks, while LayerNorm normalizes the input across the feature dimension.

Positional Encoding : We use RoPE (Rotary Positional Embedding) extended with Dynamic NTK scaling. RoPE is a powerful positional encoding method that can effectively capture the relative position information in sequences, and the Dynamic NTK scaling further enhances its ability to handle long-range dependencies.

Attention Mechanism : We leverage Flash Attention 2, which significantly reduces the computational complexity of the attention mechanism, enabling faster and more memory-efficient training, especially for long sequences.

Training Optimization We utilize DeepSpeed - Ulysess for training Transformer models with extremely long sequences. This framework is further modified and optimized based on the pipe mode.

Regarding the training settings, we set the ZERO_STAGE to 1, which helps in reducing memory usage during training by partitioning the optimizer states. We use the BF16 (Brain Floating Point 16) data type for the model parameters to speed up the training process, while the gradient accumulation data type is set to FP32 to maintain numerical stability.

Unless otherwise specified, we use cross-entropy loss as our objective function for training, which is a common choice for classification-related tasks in genomic sequence modeling.

Table 5: Model Configuration of Pretraining

Size	Sequence Length	Layers	Hidden Size	FFN Hidden Size	Num Heads	Learning Rate
6M	8192	8	256	682	8	1.00E-03
40M	8192	10	576	1536	8	6.00E-04
85M	8192	12	768	2048	12	5.50E-04
170M	8192	24	768	2048	16	5.00E-04
470M	8192	24	1280	3413	20	4.00E-04
1B	8192	24	2048	5461	32	3.00E-04
1B	30720	24	2048	5461	32	2.00E-04
1B	102400	24	2048	5461	32	1.00E-04

Data

Data Sources The *OpenGenome* dataset was composed by sampling bacterial and archaeal genomes from the GTDB v214.1, curated prokaryotic viruses from IMG/VR v4, and plasmid sequences from IMG/PR data databases.

Data Tokenization To facilitate model processing, we encode the input DNA sequences using token embedding vectors. Our vocabulary size is set to 5, consisting of the four nucleotide bases A, T, C, and G, and the special character N, which represents an unknown base. This encoding scheme transforms the biological sequences into a numerical format that can be readily processed by our model.

Pretraining Data Preparation During the pretraining phase, we adopt a masked language model (MLM) strategy. Specifically, we randomly select 15% of the tokens in the DNA sequences as masked tokens. These selected tokens are then replaced with a special <mask> token. This process allows the model to learn to predict the original nucleotides based on the context provided by the surrounding unmasked tokens.

However, since the <mask> token is typically not present in downstream fine-tuning tasks, we introduce a more sophisticated replacement rule to mitigate the inconsistency between pretraining and fine-tuning. Among the 15% of selected tokens: 1. With an 80% probability, a token is replaced with the <mask> token. To further align the long-sequence training process with downstream fine-tuning, there is a 0.02 probability that the replacement ratio can range from 0 to 80%. 2. With a 10%

probability, a token is replaced with a randomly chosen token from the vocabulary. 3. With a 10% probability, a token remains unchanged.

Sampling Strategy Inspiration for our sampling strategy is drawn from related works. Similar to using a single human reference genome and specific training and validation intervals in some studies, our approach is tailored to our integrated dataset. During training, we sample intervals from the integrated sequences and adjust the intervals at both ends to obtain sequences of length L . For the test set, we carefully select specific genomic regions to ensure the reliability of model evaluation. Although we do not follow the exact chromosome selection (chromosomes 14 and X) as in some references, we adopt a similar principle of using non-overlapping sequences of length L to evaluate the model’s performance on unseen data. This sampling strategy helps to ensure that the model is trained on diverse and representative data and can generalize well to new sequences.

Models

Table 5 presents the model configurations for the pretraining phase, comparing the settings of baseline models and our proposed TrinityDNA model.

Overall Configuration The table includes models with different parameter scales, denoted as 6M, 40M, 85M, 170M, 470M, and 1B. These models share several common structural features, such as the number of layers, hidden size, feed-forward network (FFN) hidden size, and the number of attention heads. The sequence length for most of the models is set to 8192, except for some TrinityDNA models, where the sequence lengths are 30720 and 102400.

Baseline Models For the baseline models, as the model scale increases (from 6M to 1B), the number of layers, hidden size, FFN hidden size, and the number of attention heads generally increase. Correspondingly, the learning rate decreases, which is a common practice in deep learning to reset the training process for larger models.

TrinityDNA Models The TrinityDNA models are designed to have the same basic configurations as the baselines for a fair comparison. For each model scale (e.g., 6M, 40B), the TrinityDNA model has identical hyperparameters to its corresponding baseline model in terms of sequence length, number of layers, hidden size, FFN hidden size, number of attention heads, and learning rate when the sequence length is 8192.

However, when considering the longer sequence lengths of 30720 and 102400 for the 1B TrinityDNA model, the learning rate is further reduced. This adjustment is likely to ensure stable training when dealing with much longer sequences, as longer sequences can introduce more complex dependencies and potentially lead to training instability.

C Downstream Task Details

In our study, apart from the Zero-shot benchmark, all other downstream tasks are carried out in the form of LoRA (Low-rank Adaptation) fine-tuning (Hu et al. 2021). Table 6 presents the detailed LoRA fine-tuning parameters for a variety of tasks, which is essential for understanding the specific configurations and experimental setups of each task.

LoRA Fine-tuning Parameters on GUE Benchmark (Zhou et al. 2023)

Task Descriptions

Promoter detection (Human). This task focuses on detecting proximal promoter regions, the critical genomic sequences that initiate transcription. Because these segments host numerous key regulatory elements, precise identification is essential for advancing our understanding of gene regulatory mechanisms and recognizing the genomic basis of various diseases. Following (Dreos et al. 2013), promoter sequences are split into TATA and non-TATA based on whether they contain a TATA box motif. For each subgroup, we extract the region from -249 to $+50$ base pairs around the transcription start site (TSS) to form the positive (promoter) class. For the negative (non-promoter) class, we randomly select equally sized sequences that (1) contain a TATA motif but lie outside promoter regions (TATA non-promoters), or (2) are formed by random substitutions (non-TATA non-promoters). We also merge both TATA and non-TATA subsets into a combined dataset labeled *all*.

Core promoter detection (Human). Similar to the proximal promoter task, this variant targets an even smaller window -34 to $+35$ base pairs around the TSS to capture the *core promoter* region. Predicting the core region is more challenging due to the limited context, as it concentrates on the immediate surroundings of the TSS and the start codon.

Transcription factor binding site prediction (Human). This task involves forecasting transcription factor (TF) binding sites in the human genome. TF binding sites are central to gene expression regulation; accurate prediction helps decode intricate gene regulatory networks and identify therapeutic targets. We use 690 ENCODE ChIP-seq experiments (The ENCODE Project Consortium 2012), covering 161 TF binding profiles in 91 cell lines. A 101-bp window around the center of each peak defines the positive (TFBS) class, while segments of the same length and matched GC content form the negative (non-TFBS) class. To avoid trivial or overly difficult tasks (e.g., F1 scores > 0.95 or < 0.50), we filter out such datasets and randomly pick 5 from the remaining pool.

Table 6: LoRA Fine-tuning Parameters

Task	lr	LoRA rank	LoRA alpha	batch size
tf_0	0.001	4	8	16
tf_1	0.0001	4	8	16
tf_2	0.001	4	8	16
tf_3	0.0001	4	8	16
tf_4	0.001	4	8	16
mouse_0	0.001	4	8	16
mouse_1	0.0001	24	48	16
mouse_2	0.0001	4	8	16
mouse_3	0.001	4	8	16
mouse_4	0.0001	4	8	16
core_all	0.0001	4	8	16
core_notata	0.0001	4	8	16
core_tata	0.0001	24	48	16
300_all	0.0001	24	48	16
300_notata	0.0001	8	16	16
300_tata	0.001	4	8	16
splice_reconstructed	0.0001	24	48	16
virus_covid	0.0001	4	8	16
H3	0.001	4	8	16
H3K14ac	0.001	4	8	64
H3K36me3	0.0001	96	192	16
H3K4me1	0.001	4	8	64
H3K4me2	0.001	4	8	64
H3K4me3	0.0001	48	96	16
H3K79me3	0.0005	24	48	64
H3K9ac	0.001	4	8	32
H4	0.0001	4	8	32
H4ac	0.001	4	8	32

Splice site prediction (Human). This task locates splice donor and acceptor sites in the human genome. Correct splice site identification is crucial for understanding protein diversity and the pathological effects of aberrant splicing. We use a dataset (Wang, Bai, and Chen 2019) of 400-bp sequences from the Ensembl GRCh38 reference genome. Following (Ji et al. 2021), we note that models often attain near-perfect results on the original set (10,000 splice donors, acceptors, and non-splice sites), which does not reflect the real difficulty of detecting non-canonical sites. To address this, we iteratively enrich the dataset with adversarial examples (previously unseen false positives) in a hold-out set, making the task substantially harder.

Enhancer-promoter interaction (Human). This binary classification task aims to identify whether an enhancer interacts with a promoter, a crucial relationship in the human genome that modulates gene expression. The input comprises sequence pairs (enhancer and promoter), and the output is a binary prediction indicating an interaction or lack thereof.

Species classification (Virus & Fungi). Here, the goal is to classify species based on genomic segments. We build these datasets from viral and fungal reference genomes obtained from GenBank (Benson et al. 2012).

Transcription factor binding site prediction (Mouse). Analogous to the human TFBS task, this variant deals with mouse genomes using Mouse ENCODE ChIP-seq data (Stamatoyannopoulos et al. 2012). We generate negative sequences by applying dinucleotide shuffling while preserving frequency. All other settings remain consistent with the human TFBS dataset. As with the human version, we filter out tasks with extreme F1 scores and randomly sample 5 datasets from the remaining collection.

Epigenetic marks prediction (Yeast). This task forecasts epigenetic modifications (e.g., DNA or histone modifications) in yeast. Such marks affect gene regulation without altering the DNA sequence. We downloaded 10 datasets from the following link: <http://www.jaist.ac.jp/tran/nucleosome/members.htm> and split each dataset into training, validation, and test sets at an 8:1:1 ratio.

Covid variant prediction (Virus). Focusing on SARS-CoV-2, this task predicts the virus’s variant type from 1000-bp genomic fragments. We gather data from EpiCoV (Khare et al. 2021) provided by GISAID, covering 9 variants: Alpha, Beta, Delta, Eta, Gamma, Iota, Kappa, Lambda, and Zeta.

Configurations. As shown in Tab 6, LoRA Rank and LoRA Alpha LoRA is a method used to fine-tune large pre-trained models more efficiently. The LoRA rank defines the rank of the low-rank matrices employed in the adaptation process, and LoRA alpha serves as a scaling factor. These two parameters jointly control the complexity and expressiveness of the LoRA

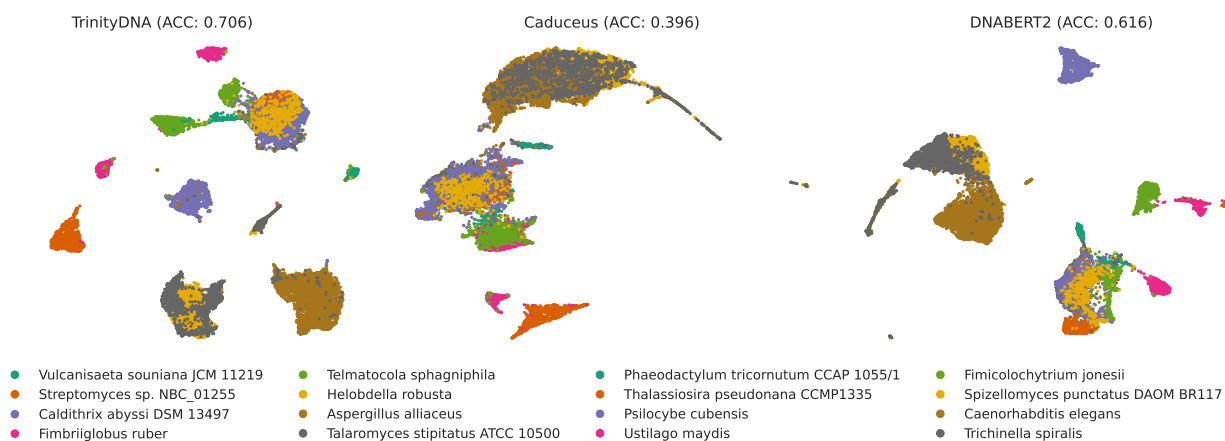


Figure 7: Zero-shot Embedding visualization of different species.

adaptation. In the table, the LoRA rank ranges from 4 to 96, and the LoRA alpha ranges from 8 to 192. Different tasks use distinct combinations of LoRA rank and LoRA alpha, suggesting that the optimal LoRA configuration depends on the characteristics of each task.

D Zero-shot Details

Datasets.

DNA pathogenicity (ClinVar). We follow the pipeline of (Nguyen et al. 2024): single-nucleotide polymorphisms (SNPs) labelled as *pathogenic* or *benign* are taken from the ClinVar release, and up to 4k nucleotide flanking windows are retrieved from the GRCh38 human reference genome to form input sequences.

RNA deep-mutational scanning (DMS). Seven non-coding RNA DMS benchmarks—*Zhang, Pitt, Hayden, Guy, Kobori, Domingo* and *Andreasson*—are collected exactly as in (Nguyen et al. 2024). They cover diverse prokaryotic RNAs.

Protein DMS. Starting from the PROTEINGYM suite (Notin et al. 2023), we keep every experiment for which the wild-type codon context can be unambiguously reconstructed. This yields nine prokaryotic sets (*Firnberg, Jacquier, Kelsic, Weeks, Rockah, Chen*) and one human set (*Sun*). To broaden the eukaryotic coverage, we further add two recently released human protein scans. For cases where the original authors reported only amino-acid sequences, we rebuild nucleic-acid inputs by selecting the most frequent codon for each amino-acid according to a codon-usage table computed from all CDS regions of GRCh38.

Zero-shot Metric Computation. For MLM-based models, we employ two metrics: (1) *Mean PPL over masked positions*: we sequentially mask token(s) and measure the resulting perplexity. (2) *Masked Mutation Impact*: We compare the PPL difference between wild-type (wt) and mutant (mt) sequences, focusing specifically on masked variant positions. For generative models such as EVO, we rely on likelihood-based scores under the same masking scheme, assessing how well the model anticipates mutations.

CDS Benchmark

Data and Configuration

Data Source. Obtain all prokaryotic reference genomes from RefSeq, and construct token-level annotation labels based on gene localization and type information in GenBank (Benson et al. 2012) annotation files.

Data Splits. *RefSeq Dataset*: We exclude the 35 training phyla, leaving 26 additional phyla in RefSeq. We randomly sample two species per phylum (or one if only one species exists), yielding 45 genomes total. These serve as an out-of-distribution test set. This benchmark tests both the model’s ability to handle very long sequences and its competence in gene structure recognition. By comparing performance on IID, metagenomic, and cross-phyla sets, we gauge the model’s robustness and generalization in realistic microbial genome annotation scenarios. The training and test data statistics are shown in Figure 9 and 10.

LoRA Tuning Setup We adopt Low-Rank Adaptation (LoRA) (Hu et al. 2021) to fine-tune our model on the CDS Benchmark. Specifically, we use a learning rate of $r = 0.001$ and a batch size of 32. For LoRA hyperparameters, we set the low-rank dimension $\text{LoRA-r} = 4$ and the scaling factor $\text{LoRA-}\alpha = 32$. Furthermore, we apply LoRA to two additional MLP layers in the classification head, whose hidden dimensions are 256 and 128, respectively. By decoupling the base model parameters

from the low-rank adaptation parameters, LoRA allows us to retain the expressive capacity of the underlying large model while conferring adaptability to new domains with minimal additional parameters.

Evaluation Metrics on the CDS Benchmark We evaluate gene annotations on the CDS Benchmark using standard metrics of recall, precision, and F_1 , where

$$\text{Recall} = \frac{\text{TP}}{\text{TP} + \text{FN}}, \quad \text{Precision} = \frac{\text{TP}}{\text{TP} + \text{FP}}, \quad F_1 = 2 \times \frac{\text{Precision} \times \text{Recall}}{\text{Precision} + \text{Recall}}.$$

Here, TP, FP, and FN represent true positives, false positives, and false negatives, respectively.

Exact Match. A predicted coding sequence (CDS) is counted as a TP under *Exact Match* if the predicted region’s start and end coordinates exactly match those of the reference annotation. In other words, the tool must recover the full CDS boundaries without offset.

75% Match. In line with (Nebrão et al. 2021), we introduce a less stringent matching criterion. Under *75% Match*, a predicted CDS is counted as a TP if:

1. The predicted CDS lies fully within the boundaries of the true (annotated) CDS.
2. The predicted CDS length is at least 75% of the length of the true CDS.
3. The predicted direction is matched.

This relaxes the exact requirement on start/end positions and instead focuses on substantially overlapping the annotated region.

E Related Work

Long-Sequence Model Transformers, with their multi-head attention, can capture such dependencies but suffer from quadratic computational complexity with sequence length, limiting their use in long-sequence tasks like genomic analysis (Devlin et al. 2018). To address this, models like BigBird use sparse attention to expand context size (Zaheer et al. 2020). Based on SSM-derived operators, a line of long-sequence models is proposed to handle long DNA sequences (up to 1M bps) but is unidirectional and not robust to RC inputs (Liu et al. 2024b; Poli, Suteu et al. 2023; Liu et al. 2024c; Nguyen et al. 2024).

DNA Foundation Model Early DNA language models such as DNABERT were restricted by Transformer’s complexity, with limited context sizes for DNA sequences (Ji et al. 2021; Zhou et al. 2023; Dalla-Torre et al. 2023; Nguyen et al. 2023; Li et al. 2024). Recent research focuses on integrating biological features. Caduceus (MambaDNA) exploits DNA’s reverse-complement symmetry for better gene regulation modeling (Mallet and Vert 2021). Our TrinityDNA model innovatively adds the Groove Fusion module to capture DNA structural features. In training, traditional models on single-type genomic data have limited generalization. Our evolutionary training strategy, with staged training on different genomes and increasing context lengths, enhances model adaptability and performance.

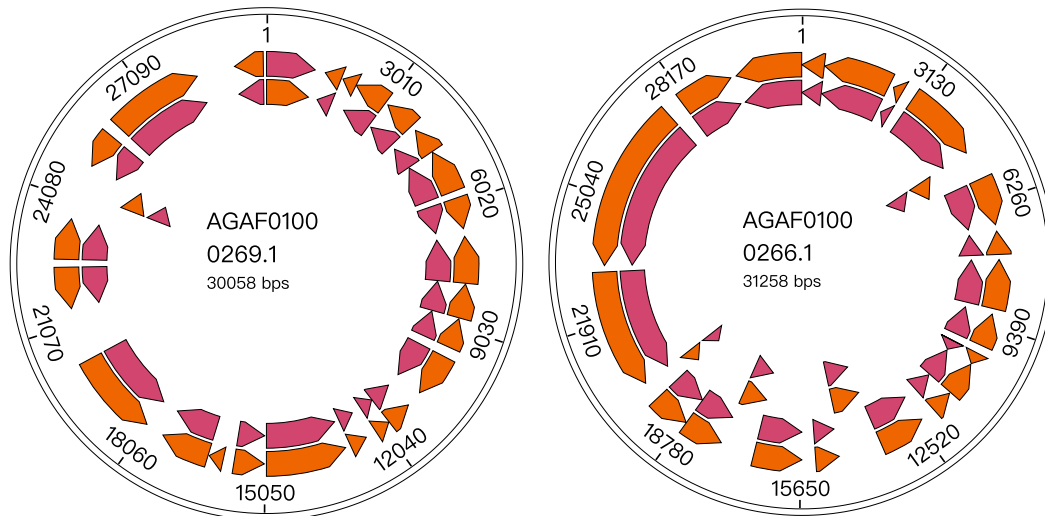


Figure 8: Comparison diagrams of two examples in the CDS annotation task. The orange parts represent the annotation results of Prodigal (serving as the ground truth), and the red parts represent the prediction results of TrinityDNA.

Annotation - Train Set

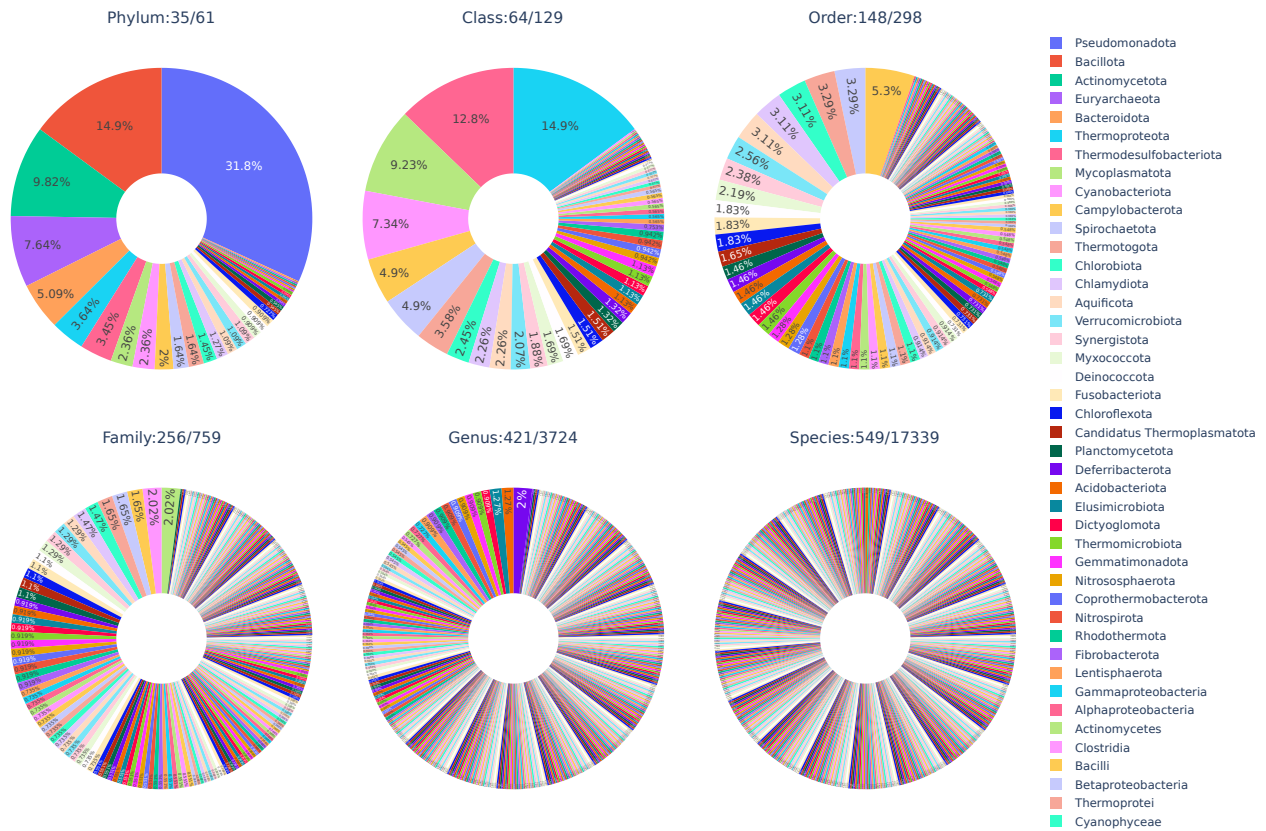


Figure 9: Distribution of taxonomic groups in the training and IID test sets. Our benchmark datasets are constructed from a comprehensive collection of bacterial and archaeal genomes (17,339 genomes across 61 phyla). From these, we selected 35 phyla for training, and the IID test set is randomly sampled from these training phyla, maintaining the same taxonomic distribution. This design enables evaluation of the model's ability to generalize within known taxonomic groups.

Annotation - Test Set



Figure 10: Distribution of taxonomic groups in the OOD test sets. To evaluate model generalization beyond the training distribution, we constructed two distinct OOD test sets: A phylogenetically diverse set of 45 genomes carefully selected from the remaining phyla not used in training, ensuring maximum coverage of untrained phyla.

Impact Statements

The work presented in this paper introduces TrinityDNA, a novel deep-learning model designed to address key challenges in DNA sequence modeling. By incorporating biologically informed components such as Groove Fusion and Gated Reverse Complement (GRC), along with a multi-scale attention mechanism and evolutionary training strategy, TrinityDNA makes significant strides in improving the accuracy and efficiency of genomic sequence analysis.

The impact of TrinityDNA extends beyond academic research in computational genomics. The model's ability to efficiently capture long-range dependencies in DNA sequences enables more accurate predictions of gene functions, regulatory mechanisms, and other biological insights. This can have profound implications for various fields, including personalized medicine, where understanding genetic variations is crucial for disease prevention and treatment. In addition, by improving the understanding of complex biological systems, TrinityDNA could accelerate advancements in biotechnology and drug development, where genomic data plays a pivotal role in identifying novel therapeutic targets and biomarkers.

Furthermore, the model's scalability and integration of multi-species genomic data position it as a tool with the potential to advance our understanding of the genomic underpinnings of diverse organisms. This has wide-reaching implications for evolutionary biology, conservation efforts, and the study of microbiomes, where large-scale comparative genomic analysis is essential. By bridging the gap between computational methods and biological insights, TrinityDNA serves as a significant step toward more robust, data-driven approaches to understanding the complexities of life at the genomic level.